Hydrogen Production Catalysts

Deutsche Ausgabe: DOI: 10.1002/ange.201507626
Internationale Ausgabe: DOI: 10.1002/anie.201507626

Nanosized IrO_x–Ir Catalyst with Relevant Activity for Anodes of Proton Exchange Membrane Electrolysis Produced by a Cost-Effective Procedure

Philipp Lettenmeier, Li Wang, Ute Golla-Schindler, Pawel Gazdzicki, Natalia A. Cañas, Michael Handl, Renate Hiesgen, Seyed S. Hosseiny, Aldo S. Gago, and Kaspar A. Friedrich*

Abstract: *We have developed a highly active nanostructured iridium catalyst for anodes of proton exchange membrane (PEM) electrolysis. Clusters of nanosized crystallites are obtained by reducing surfactant-stabilized $IrCl_3$ in water-free conditions. The catalyst shows a five-fold higher activity towards oxygen evolution reaction (OER) than commercial Ir-black. The improved kinetics of the catalyst are reflected in the high performance of the PEM electrolyzer (1 $mg_{Ir}cm^{-2}$), showing an unparalleled low overpotential and negligible degradation. Our results demonstrate that this enhancement cannot be only attributed to increased surface area, but rather to the ligand effect and low coordinate sites resulting in a high turnover frequency (TOF). The catalyst developed herein sets a benchmark and a strategy for the development of ultra-low loading catalyst layers for PEM electrolysis.*

The total global hydrogen production value is greater than 30 million tons and governed mainly by the demand of the ammonia manufacturing and petrochemical industries.[1] On a less prominent scale, but with increasing interest, other industries have recognized the value of hydrogen as an energy carrier, as well as one of the main educts to synthesize liquid fuels, for example, by catalytic hydrogenation of CO_2.[2,3] However, around 90% of the global hydrogen production is generated by reforming hydrocarbons, which is associated with a significant carbon footprint.[4] The dilemma facing industry and research is that current hydrogen-producing technologies with zero carbon footprints generally have a low production value, unsatisfying efficiencies, high maintenance needs, or are simply too expensive to compete with the state of the art technologies.[5,6]

Water electrolysis represents one of numerous environmentally friendly, but at present economically unattractive, technologies. At low temperatures, this process can take place in various electrochemical devices and chemical environments, among which alkaline and proton exchange membrane electrolyzers have proved to be interesting for future high volume hydrogen production. While alkaline electrolyzers are advantageous with respect to their longevity and costs, the lack in gas purity, safety, and response time has pushed the research and industrial interests towards proton exchange membrane (PEM) electrolysis in the recent years.[7,8]

For water splitting in PEM electrolyzers, the choice of the oxygen evolution reaction (OER) catalyst employed at the anode has a profound impact on the cost, lifetime, and efficiency of the device. Iridium is commonly used as a OER catalyst, but is highly priced ($546 per troy ounce)[9] and one of the rarest elements in the earth crust, with an annual production and consumption value of only about 4 to 9 tons.[10–12] Several approaches have been proposed to overcome the challenges associated with the precious metal OER catalyst such as reducing the particle size, thereby increasing the surface to mass ratio,[13] using electro-ceramic supports,[14,15] or enhancing the phase structure.[16] These characteristics can be modified through different approaches, while a direct modification during synthesis without post-treatment represents an attractive way to reduce production costs influencing the commercialization of future catalysts. Recently, Tran et al. proposed a way for reducing the iridium content by doping oxide films with silicon, rendering a very high TOF for OER.[17]

One of the major reasons for the slow progress in finding improved catalysts for OER electrocatalysis is that the selection of these materials has been guided mainly by theoretical-based approaches such as ab-initio density functional theory (DFT) calculations.[18,19] This seems to become a critical issue in electrochemistry,[20] and while theoretical approaches are an important and powerful tool, synthesis steps with a trial and error route are indispensable to achieve better catalysts for industrial PEM electrolyzers. Nonetheless, a purely theoretical approach will enhance the catalyst development in a timely manner.

[*] P. Lettenmeier, L. Wang, Dr. P. Gazdzicki, N. A. Cañas, Dr. S. S. Hosseiny, Dr. A. S. Gago, Prof. Dr. K. A. Friedrich
Institute of Engineering Thermodynamics
German Aerospace Center (DLR)
Pfaffenwaldring 38–40, 70569 Stuttgart (Germany)
E-mail: aldo.gago@dlr.de
M. Handl, Prof. Dr. R. Hiesgen
University of Applied Sciences Esslingen
Department of Basic Science
Kanalstrasse 33, 73728 Esslingen (Germany)
Dr. U. Golla-Schindler
Group of Electron Microscopy of Materials Science
Central Facility for Electron Microscopy
University of Ulm
89081 Ulm (Germany)

Supporting information for this article is available on the WWW under http://dx.doi.org/10.1002/anie.201507626.

The system $Ir_xRu_{1-x}O_2$ ($0 \le x \le 1$) has been considered the most advanced catalyst for OER for more than four decades.[7] Marshall et al. developed an extensive variety of metal mixed oxides (MOX) with the purpose of reducing the loading of Ir and improving stability of Ru.[21] Earlier, the pioneering works of Trasatti and co-workers explored these materials for manufacturing dimensional stable anodes (DSA).[22] However, thermal treatment is required to produce a dense layer of the active material on titanium substrates. Conversely, nanosized Ru[23] and Ir[24,25] have been recently explored, revealing mass activities far greater than the oxide counterparts.

The primary goal of this communication is to reveal the physical and electrochemical properties of an OER catalyst synthetized by a simple and efficient method, and comparing it with Ir-black. We have deliberately chosen Ir-black as the benchmark catalyst as it has a similar structure and surface properties to our material. This work also aims to understand the reasons for the superior activity of the developed material, fostering further research into the OER mechanism on electrochemically oxidized iridium catalysts with a metallic core and large surface area.

The catalyst, with an iridium oxide surface and metallic iridium base (IrO_x-Ir) was synthesized by reducing surfactant-stabilized $IrCl_3$ in anhydrous ethanol at room temperature. Details of the synthesis procedure are given in the Supporting Information. X-ray photoelectron spectroscopy (XPS) studies of IrO_x-Ir and Ir-black show that both contain similar amounts (ca. 85 at%) of metallic iridium after removal of surface contaminations by sputtering (Figure 1 a,c). However, the surface compositions are different. Figure 1 b and d show the concentration profiles of the individual components identified in the samples. Evidently, the surface of the IrO_x-Ir sample exhibits carbon and chlorine contamination, as well as an increased concentration of oxygen. These contaminants are most probably due to unreduced $IrCl_3$, which has been observed by X-ray diffraction (XRD; Figure 1 e), while Ir-black (Figure 1 f) is pristine. It was not possible to completely remove the contaminant, even after the cleaning procedure. Less than 3 wt% of Cl is still present even after electrochemical characterization, as confirmed by energy dispersive X-ray (EDX) analysis performed on the catalyst layer (Supporting Information, Table S3). The traces of $IrCl_3$ could lead to Cl_2 evolution, which would be detrimental for the coated interconnectors of the PEM electrolyzer. Further characterization, with techniques such as differential electrochemical mass spectrometry (DEMS), is required to find out how much Cl_2 is evolved during OER over time.

Carbon impurities in IrO_x-Ir could be identified as surfactant residuals by analyzing the washing solution following purification. The oxide species were determined by fitting the first level spectrum (0 s; Figure 1 a,c) using the metallic reference and a synthetic doublet of symmetric peaks with 3 eV separation and a fixed height and width ratio. The outcome of this fit is an oxide species with the $Ir4f_{7/2}$ level located at 62.2 eV, which has been used to fit the Ir4f spectra of all other sputtering levels of the XPS depth profile. Applying this method, both samples showed an increased concentration of oxygen (ca. 30–40%) that rapidly decreases upon sputtering. However, no iridium oxide could be detected on the surface of the Ir-black sample.

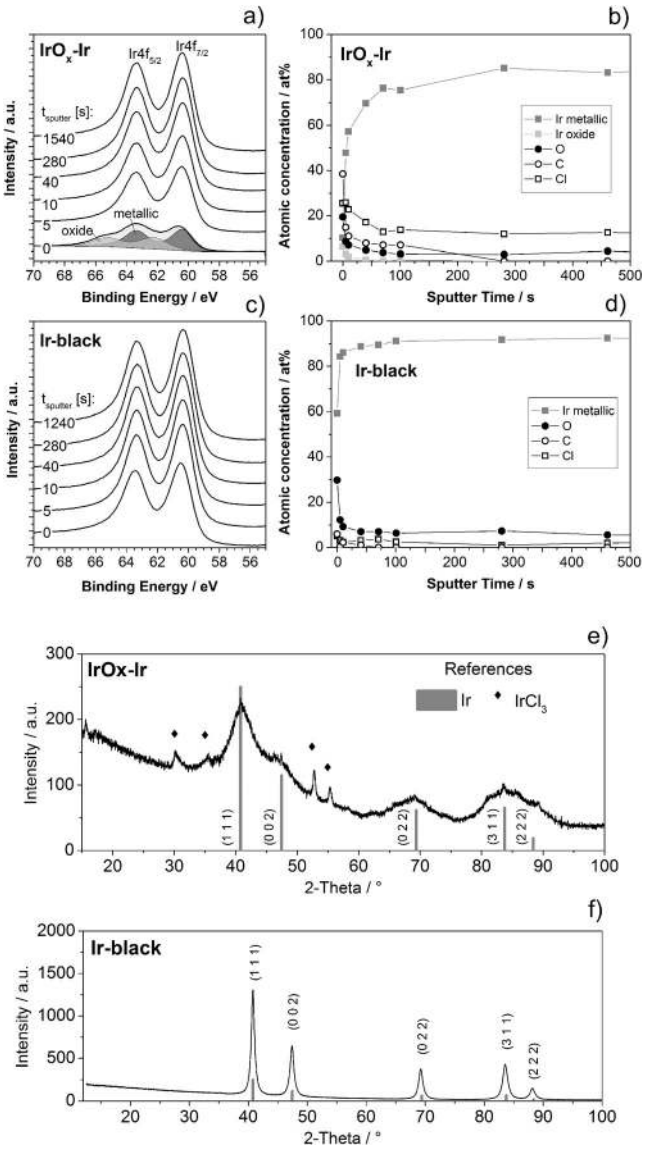

Figure 1. XPS analysis of IrO_x-Ir and Ir-black. Panels a) and b) depict 4f detailed spectra of IrO_x-Ir and a concentration profile of identified components, respectively. Analogous measurements for the Ir-black sample are provided in c) and d). X-ray diffraction patterns of synthetized e) IrO_x-Ir and commercial f) Ir-black. Ir reflection markers (ICDD 03-065-1686) and difference curve are provided on the bottom of the figure. Diamond-shape symbols correspond to $IrCl_3$ that was neither reduced nor dissolved after the synthesis procedure.

Transmission electron microscopy (TEM) pictures (Figure 2 a,b) show agglomerated and randomly oriented IrO_x-Ir particles and Ir-black sheet-like agglomerates, respectively. The crystallite size of IrO_x-Ir was measured to be in the range of approximately 2 nm, while Ir-black consists of much larger particles ranging from 100 to 500 nm. These results are in good agreement with the Rietveld refined analysis carried out from the XRD measurements (Supporting Information).

High-resolution TEM pictures show for both catalysts a lattice plane distance of 2.23 Å, in agreement with the

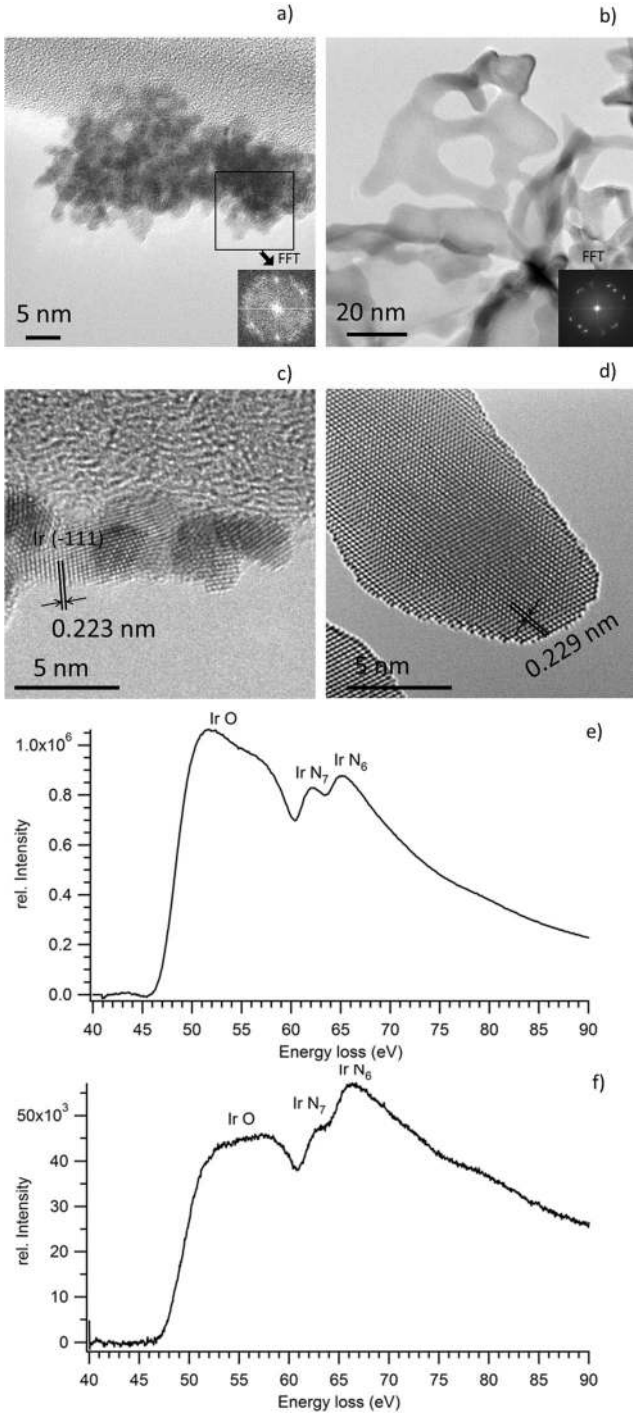

Figure 2. TEM micrographs and power-law background subtracted EELS spectra of IrO_x-Ir and Ir-black. a, b) Overview images show a) cluster of IrO_x-Ir, inset FFT of the selected area b) Ir-black particles inset FFT of the whole image area. c, d) HRTEM images and e, f) correlated EELS of IrO_x-Ir and Ir-black, respectively.

theoretical (111) lattice plane distance of 2.24 Å (Figure 2c,d). Electron energy loss spectroscopy (EELS) investigations were performed to gain more information about the structure. The EELS studies of the IrO_x-Ir particles solely delivered Ir. The electron loss near-edge structure enables the separation of IrO, with a first peak position at roughly 51.5 eV and a shoulder at 56.5 eV, and the $IrN_{6,7}$-edges, with a peak position at 62 eV and 65 eV for the N_7 and N_6 transitions, respectively. The significant differences in the peak height and peak shapes for IrO_x-Ir and Ir-black indicate a change in the electronic environment of Ir, such as the valence state, coordination, bonding, and crystal distortion.

When starting our electrochemical characterization, we found it necessary to address whether our catalyst should be iridium oxide because XPS revealed it to have an oxide layer. To determine this, we investigated the adsorption of carbon monoxide in a CO-stripping experiment (Figure S7). Although CO-stripping is a powerful technique for measuring the electrochemical surface area of Pt-based PEM fuel cell catalysts,[26,27] it is misleading for determining this parameter for OER catalysts because the chemisorption properties are different depending on the degree of oxidation.

Figure 3a compares the current-potential response of IrO_x-Ir and Ir-black in argon-saturated 0.5 M H_2SO_4 electrolyte. Here, IrO_x-Ir shows almost five- and eleven-times higher activity than Ir-black (1.6 $A\,g^{-1}$) and thermally oxidized commercial IrO_2 (0.74 $A\,g^{-1}$; Inset, Figure S7), respectively at 0.25 V overpotential, 25 °C in 0.5 M H_2SO_4. Marshall et al. produced IrO_2 by thermal decomposition of iridium salt on a titanium-support, achieving 2 $A\,g^{-1}_{oxide}$ in 0.5 M H_2SO_4.[28] In comparison to a recent report on IrO_2 nanoparticles,[29] IrO_x-Ir is 6 $A\,g^{-1}$ higher. Initially, this enhancement may be explained by the smaller crystallite size, and thus higher Brunauer-Emmett-Teller (BET) surface area of IrO_x-Ir (59 $m^2\,g^{-1}$) compared to Ir-black (18 $m^2\,g^{-1}$). Furthermore, from atomic force (AFM) analysis on the catalyst layer deposited on the RDE, the mean particle size in the electrode is about ten-times smaller for IrO_x-Ir than for Ir-black. However, other factors, such as the oxidation mechanism of iridium and TOF, are a central part of the OER path.[30,31]

We evaluated the TOF to gain more information about the intrinsic properties and ensure that the higher activities can be correlated with the actual OER.[32,33] This parameter was determined from the redox surface sites Ir^{III}/Ir^{IV} (Figure S10). Figure 3b shows the TOF measurements of IrO_x-Ir and Ir-black with respect to the overpotential obtained from the redox surface sites. The high TOF of IrO_x-Ir accounts for the relatively low number of active sites and high specific activity.[13]

The kinetic properties of the catalysts were evaluated by extrapolating Tafel curves to the thermodynamic reversible potential. The resulting exchange current densities were investigated and depicted in Figure 3c. It is important to note that the linear fit of the exchange current density of IrO_x-Ir has a lower slope over measured temperature than the one of Ir-black, corresponding to a lower activation energy. The calculated activation energy for IrO_x-Ir and Ir-black is 40 $kJ\,mol^{-1}$ and 52 $kJ\,mol^{-1}$, respectively. Both values are consistent with other reports.[34–36] Based on the activation energies, the transfer coefficient (α) values were calculated to evaluate the rate-determining steps according to Krasil'shchikov.[37] The following equations (1–4) represent the possible determining steps, where S corresponds to the active site of the catalytic metal.

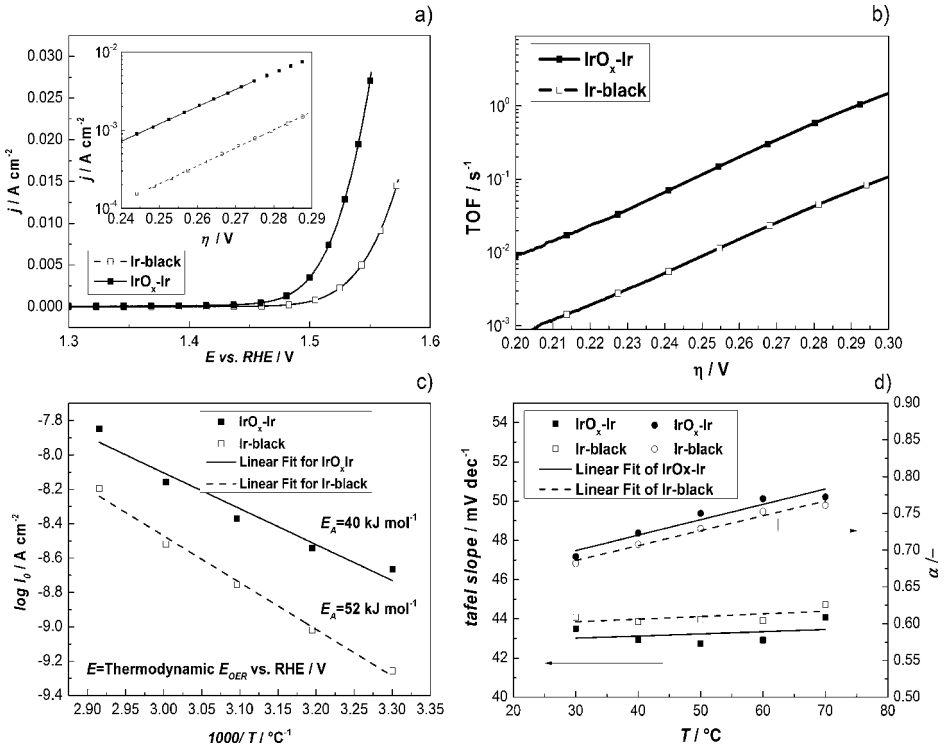

Figure 3. a) Current-potential curves of IrO_x-Ir and Ir-black with inset showing the Tafel slopes versus overpotential at 25 °C and sweep rate of 5 $mV s^{-1}$, rotation speed of 2500 rpm, in argon-saturated 0.5 M H_2SO_4. b) TOF vs. overpotential of IrO_x-Ir and Ir-black determined from the anodic Ir^{III} to Ir^{IV} oxidation charge CV. c) Arrhenius plots at 1.23 V versus RHE of IrO_x-Ir and Ir-black. The corresponding temperature dependence of the Tafel slope (β) and transfer coefficient (α) is shown in (d).

$$S + H_2O \rightarrow S\text{-}OH + H^+ + e^- \quad (1)$$

$$S\text{-}OH \rightarrow S\text{-}O^- + H^+ \quad (2)$$

$$S\text{-}O^- \rightarrow S\text{-}O + e^- \quad (3)$$

$$S\text{-}O + S\text{-}O \rightarrow O_2 + 2S \quad (4)$$

Figure 3 d shows the α values for both catalysts. The Tafel slopes were also determined to be between 43.7–44.7 $mV dec^{-1}$, indicating a rate-determining step according to Equation (3) for overpotentials between 250 to 300 mV.[37] The slope equation of 2.303 (2RT/3F) could also fit for the second electron transfer of the electrochemical path described by Bockris.[38] Values above the theoretical value can be explained by the compactness of the layer.[34]

Based on Pourbaix diagrams of iridium in a water system, the metal must be oxidized in acid media. This can be supported by the appearance of anodic peaks observed between 0.6 and 1.0 V in the surface oxidation with the opening window cyclic voltammogram (CV; Figure S11). Furthermore, the measured Tafel slope is a common value for iridium-based catalysts. We performed XPS measurements on the catalyst layer after electrochemical measurements, and we found out that our working electrode is a form of metal oxide rather than metal after water oxidation (Figure S3). However, the mixed valence and metallic core are still present. The real nature of the catalyst during water oxidation can only be elucidated with advanced in-operando techniques, such as ambient pressure XPS or extended X-ray absorption fine structure (EXAFS), which go beyond the scope of this communication.

Membrane electrode assemblies (MEA) with Ir-black and IrO_x-Ir were produced by wet spraying to investigate the catalyst performance in a PEM electrolyzer. Figure 4 shows the performance of both catalysts in a 25 cm^2 PEM electrolysis cell. Clearly, a shift to the lower potential range can be observed for IrO_x-Ir, and consequently an improvement in efficiency. The inset in Figure 4 depicts the Nyquist plots of electrochemical impedance spectroscopy (EIS) for Ir-black and IrO_x-Ir. A reduction of the central semi-cycle, related to the anode charge transfer process, confirmed the improved catalytic activity of IrO_x-Ir. Stability tests (Supporting Information) showed negligible degradation after 100 h of

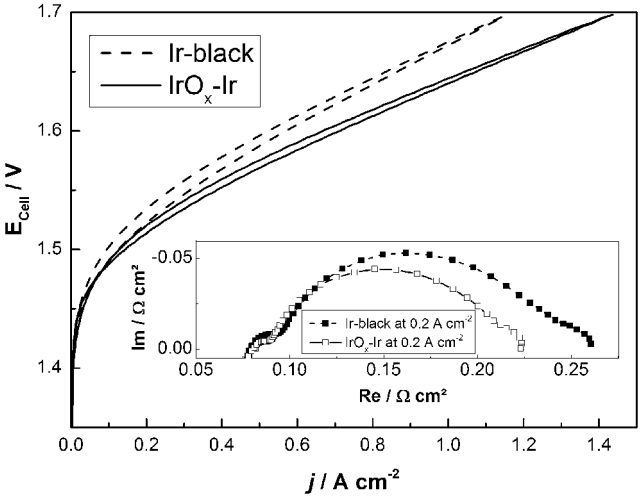

Figure 4. Polarization curves of a 25 cm^2 PEM electrolysis cell at a scan rate of 5 $mV s^{-1}$ at 80 °C. The MEA was produced by wet spraying inks with 1 $mg cm^{-2}$ IrO_x-Ir and 1 $mg cm^{-2}$ Pt/C on Nafion 212. The inset shows the EIS at 0.2 $A cm^{-2}$ with a frequency range of 100 kHz–50 mHz at 80 °C.

operation under nominal conditions (2 $A cm^{-2}$, 80 °C). However, for practical applications, long-term durability tests of more than 1000 h are required to determine the longevity of Ir-IrO_x. Despite having a highly active anode, the performance of Ir-IrO_x in the PEM electrolyzer does not yet match

the state-of-the art.[39] Optimizing the MEA manufacturing process, cell components, and measuring system, as well as long-term stability tests are all part of our on-going work.

In this communication, we presented a facile synthesis method of a iridium catalyst with a electrochemically oxidized surface on a metallic core for electrochemical water splitting. The procedure is environmentally friendly, cost effective, and scalable for large production. Our material shows higher activity than commercially available Ir-black. We demonstrated that this superior activity can be attributed to the higher intrinsic exchange current densities, while the effect of an increased surface area is less predominant and double layer capacitance is moderate. Further strategies for understanding the character of the IrO_x-Ir catalyst are needed. In this context, we encourage further interest from the scientific community on electrochemically-oxidized OER catalysts with metallic cores, which could reduce the cost of PEM electrolysis technology for a sustainable hydrogen economy.

Acknowledgements

The authors acknowledge the German Federal Ministry for Economic Affairs and Energy (BMWi) for financial support in the project No. 0325440A. The authors are also grateful to Anke Steinhilber, Indro Biswas for further XPS analysis, and Noriko Metzger-Sata for performing BET measurements.

Keywords: electrocatalysts · iridium · oxygen evolution reactions · proton exchange membranes

How to cite: *Angew. Chem. Int. Ed.* **2016**, *55*, 742–746
Angew. Chem. **2016**, *128*, 752–756

[1] R. R. Schrock, *Proc. Natl. Acad. Sci. USA* **2006**, *103*, 17087.
[2] N. Armaroli, V. Balzani, *ChemSusChem* **2011**, *4*, 21–36.
[3] G. A. Olah, G. K. S. Prakash, A. Goeppert, *J. Am. Chem. Soc.* **2011**, *133*, 12881–12898.
[4] S. J. Davis, K. Caldeira, H. D. Matthews, *Science* **2010**, *329*, 1330–1333.
[5] S. Sharma, S. K. Ghoshal, *Renewable Sustainable Energy Rev.* **2015**, *43*, 1151–1158.
[6] P. Parthasarathy, K. S. Narayanan, *Renewable Energy* **2014**, *66*, 570–579.
[7] M. Carmo, D. L. Fritz, J. Mergel, D. Stolten, *Int. J. Hydrogen Energy* **2013**, *38*, 4901–4934.
[8] J. Eichman, K. Harrison, M. Peters, *Novel Electrolyzer Applications: Providing More Than Just Hydrogen*, National Renewable Energy Laboratory, Technical Report NREL/TP-5400-61758, **2014**.
[9] National Minerals Information Center, "Mineral Industry Surveys", **2015**.
[10] C. Hagelüken, *Metall 60. Jahrgang* **2006**, *1–2*, 31–42.
[11] G. B. Haxel, J. B. Hedrick, G. J. Orris, *USGS Fact Sheet 087-02*, **2002**.
[12] P. C. K. Vesborg, T. F. Jaramillo, *RSC Adv.* **2012**, *2*, 7933.
[13] E. a. Paoli, F. Masini, R. Frydendal, D. Deiana, C. Schlaup, M. Malizia, T. W. Hansen, S. Horch, I. E. L. Stephens, I. Chorkendorff, *Chem. Sci.* **2015**, *6*, 190–196.
[14] H.-S. Oh, H. N. Nong, T. Reier, M. Gliech, P. Strasser, *Chem. Sci.* **2015**, *6*, 3321–3328.
[15] H. N. Nong, H.-S. Oh, T. Reier, E. Willinger, M.-G. Willinger, V. Petkov, D. Teschner, P. Strasser, *Angew. Chem. Int. Ed.* **2015**, *54*, 2975–2979; *Angew. Chem.* **2015**, *127*, 3018–3022.
[16] R. D. L. Smith, M. S. Prévot, R. D. Fagan, Z. Zhang, P. A. Sedach, M. K. J. Siu, S. Trudel, C. P. Berlinguette, *Science* **2015**, *340*, 60–63.
[17] V.-H. Tran, T. Yatabe, T. Matsumoto, H. Nakai, K. Suzuki, T. Enomoto, T. Hibino, K. Kaneko, S. Ogo, *Chem. Commun.* **2015**, *51*, 12589–12592.
[18] N. B. Halck, V. Petrykin, P. Krtil, J. Rossmeisl, *Phys. Chem. Chem. Phys.* **2014**, *16*, 13682–13688.
[19] J. Rossmeisl, a. Logadottir, J. K. Nørskov, *Chem. Phys.* **2005**, *319*, 178–184.
[20] W. Schmickler, S. Trasatti, *J. Electrochem. Soc.* **2006**, *153*, L31.
[21] A. Marshall, S. Sunde, M. Tsypkin, R. Tunold, *Int. J. Hydrogen Energy* **2007**, *32*, 2320–2324.
[22] S. Trasatti, *Electrochim. Acta* **2000**, *45*, 2377–2385.
[23] See Ref. [13].
[24] T. Reier, M. Oezaslan, P. Strasser, *ACS Catal.* **2012**, *2*, 1765–1772.
[25] H. N. Nong, L. Gan, E. Willinger, D. Teschner, P. Strasser, *Chem. Sci.* **2014**, *5*, 2955.
[26] K. Friedrich, F. Henglein, U. Stimming, W. Unkauf, *Electrochim. Acta* **2000**, *45*, 3283–3293.
[27] F. Maillard, M. Eikerling, O. V. Cherstiouk, S. Schreier, E. Savinova, U. Stimming, *Faraday Discuss.* **2004**, *125*, 357.
[28] A. Marshall, B. Børresen, G. Hagen, M. Tsypkin, R. Tunold, *Energy* **2007**, *32*, 431–436.
[29] Y. Lee, J. Suntivich, K. J. May, E. E. Perry, Y. Shao-Horn, *J. Phys. Chem. Lett.* **2012**, *3*, 399–404.
[30] S. Trasatti, *Electrochim. Acta* **1984**, *29*, 1503–1512.
[31] A. Minguzzi, O. Lugaresi, E. Achilli, C. Locatelli, A. Vertova, P. Ghigna, S. Rondinini, *Chem. Sci.* **2014**, *5*, 3591.
[32] H. N. Nong, L. Gan, E. Willinger, D. Teschner, P. Strasser, *Chem. Sci.* **2014**, *5*, 2955–2963.
[33] C. P. P. De Pauli, S. Trasatti, *J. Electroanal. Chem.* **1995**, *396*, 161–168.
[34] G. Lodi, E. Sivieri, A. Debattisti, S. Trasatti, *J. Appl. Electrochem.* **1978**, *8*, 135–143.
[35] T. Audichon, E. Mayousse, T. W. Napporn, C. Morais, C. Comminges, K. B. Kokoh, *Electrochim. Acta* **2014**, *132*, 284–291.
[36] a. K. M. Fazle Kibria, S. a. Tarafdar, *Int. J. Hydrogen Energy* **2002**, *27*, 879–884.
[37] a) A. Damjanovic, A. Dey, J. O. Bockris, *J. Electrochem. Soc.* **1966**, *113*, 739; b) A. I. Krasil'shchikov. *Zh. Fiz. Khim.* **1963**, *37*, 531–537.
[38] J. O. Bockris, T. Otagawa, *J. Phys. Chem.* **1983**, *87*, 2960–2971.
[39] H. Su, V. Linkov, B. J. Bladergroen, *Int. J. Hydrogen Energy* **2013**, *38*, 9601–9608.

Received: August 14, 2015
Revised: October 28, 2015
Published online: November 24, 2015

